Optimization of ion acceleration in the interaction of intense femtosecond laser pulses with ultrathin foils

Q. L. Dong,[1] Z.-M. Sheng,[1] M. Y. Yu,[2] and J. Zhang[1,*]
[1]*Laboratory of Optical Physics, Institute of Physics, Chinese Academy of Sciences, Beijing 100080, People's Republic of China*
[2]*Institut für Theoretische Physik I, Ruhr Universität Bochum, D-44780 Bochum, Germany*
(Received 22 August 2002; revised manuscript received 27 February 2003; published 19 August 2003)

Ion emission is investigated using particle-in-cell simulations where a Gaussian laser pulse with duration 50 fs and intensity 1.37×10^{19} W/cm^2 is incident obliquely onto ultrathin solid foils. When the foil is thicker than 0.1 μm, it is opaque to the laser light and the highest ion energy drops exponentially with target thickness. Optimization of ion acceleration occurs for a target with a thickness of 0.04 μm when it becomes transparent to the laser light. The behaviors of the high-energy electrons oscillating in the charge separation potential at the front and the rear of the target, as well as the enhanced electron acceleration in the laser pulse, play dominant roles for the observed features of ion emission. The relation of the optimal target thickness with parameters of the incident laser pulse and foil targets is also discussed.

DOI: 10.1103/PhysRevE.68.026408 PACS number(s): 52.38.Kd, 52.25.Tx, 52.50.Jm, 52.65.Rr

I. INTRODUCTION

Energetic electrons and ions generated in the interaction of ultrashort intense laser pulses with plasmas is of much interest because of their many potential applications. The interaction depends greatly on the parameters of the laser pulse, such as the intensity, wavelength, light polarization, pulse duration, etc. [1]. The initial plasma state, for example, the density profile, can also significantly affect the laser-plasma interaction process. Suitable plasmas can be produced by introducing a prepulse with a proper time delay to the main pulse [2] or by using targets with specific features [3–7]. Attempts to realize compact electron/proton accelerators and neutron sources are based on the interaction of ultrashort laser pulses with targets such as clusters, thin foils, etc. [4]. By using clusters, Ditmire *et al.* [5] observed enhanced laser absorption and x-ray emission. The electron acceleration was found to be related to the laser polarization, and the ion emission was almost isotropic [6]. The latter is different from the results by Kumarappan *et al*., who found that the emission of ions with higher ionization states is preferable in the laser polarization direction [7]. Although one can obtain MeV ions from the cluster target, collimated ion beams would be preferable for most applications. Such ion beams can be obtained by using a planar solid target [3]. Many existing works considered the effects of target thickness on proton acceleration, which is related to the number, the effective temperature, and the spatial distribution of the hot electrons produced during the interaction. Maksimchuk *et al.* [3] found that thin foils with a thickness of 10 μm is optimal for proton acceleration. This was attributed to the enhanced electrostatic field arising from increased deposition of the most energetic electrons in the solid target. On the other hand, Mackinnon *et al.* [3] observed no optimal thickness, but the highest proton energy drops linearly as the target thickness is increased from 3 to 10 μm, and then a plateau region appears. Differences between the two experiments mentioned above are believed to be due to the greatly different contrast ratio, the duration, and the intensity of the laser pulses applied. The common character between them is that the short laser pulse interacts only with the material in the front of the target, which is less than the laser wavelength. Energy transport from the laser-produced plasma to the rest of the solid target [8] significantly reduces the plasma temperature and can therefore prevent the ions from achieving higher energies. This effect can be eliminated by using ultrathin solid foils of sub-micrometer thickness.

In this paper, we use particle-in-cell (PIC) simulations to investigate the optimal conditions for the ion acceleration in the laser interactions with thin foils. We demonstrate that, by using an ultrathin foil, ions with energies up to tens of MeV can be produced within a very narrow spread angle around the normal direction of the target. Different from Maksimchuk *et al.* and Mackinnon *et al.* [3], we found that the optimal foil thickness for the ion acceleration is about several times of the effective skin depth when the foil is transparent to the laser pulse. The increased hot electron number and increased effective temperature due to the foil transparency are found to be responsible for the optimization behavior of the ion emission. When the target thickness increases and becomes opaque to the laser, the highest energy of the emitted ions decreases exponentially.

II. PIC SIMULATION RESULTS

Our PIC code is a 1D3V one, which can include the binary collisions between electrons and ions with a scheme given in Ref. [9]. Typically in simulations to be shown in the following, the simulation box has a dimension of 20 laser wavelengths, with the aluminum plasma foil located in the middle. The simulation box is divided into 100 000 cells, with maximally 200 electrons and ions in each cell in plasma initially. The thickness of foils varies from 0.01 μm to 15 μm. The initial plasma profile is assumed to be a homogeneous slab with the electron density of $n_{e0}=100n_c$, where

*Author to whom correspondence should be addressed.
Email address: jzhang@aphy.iphy.ac.cn

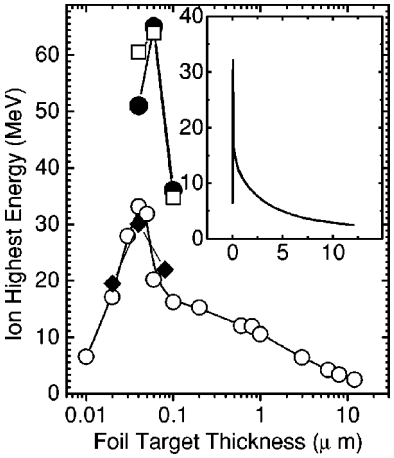

FIG. 1. Highest ion energy versus the foil thickness for three different *p*-polarized laser pulses incident at 45 ° to the target normal: (i) the open-circle line for 1.37×10^{19} W/cm^2, 50-fs laser; (ii) the solid-circle line for 3.5×10^{19} W/cm^2, 50-fs laser; (iii) the square line for 1.37×10^{19} W/cm^2, 100-fs laser. The diamond-line is obtained for case (i) taking into account the binary-collision effect in the PIC code. The inset is also the dependence of the highest ion energy on target thickness for case (i), except for linear abscissa.

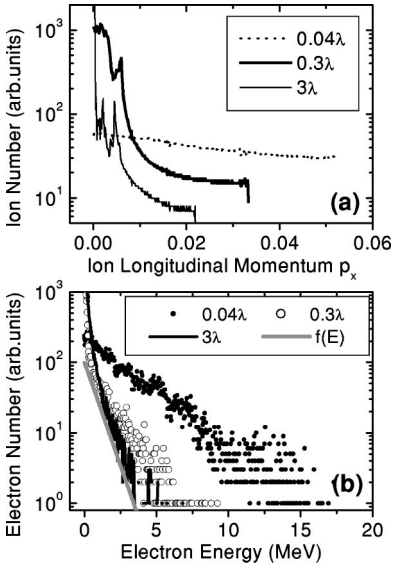

FIG. 2. (a) Ion momentum distribution for the laser pulse (i) and three target thicknesses: 0.04 μm, 0.3 μm, and 3 μm. (b) Electron energy distribution. The simulation parameters are the same as in (a). The gray line shows the Maxwellian distribution $f(E)=100\exp[-E/0.74\ (\mathrm{MeV})]$.

n_c is the critical electron density, which is about 1.1×10^{21} cm^{-3} for the laser wavelength of 1 μm. The initial temperatures of electrons and ions were both set to zero, since the numerical self-heating is very limited during a short time duration such as a few hundred femtoseconds. Meanwhile, the level of the self-heating is much lower than the electron temperature gained from the relativistic laser-plasma interactions according to our PIC simulations. A Gaussian laser pulse either *p* or *s* polarized is incident on aluminum foil targets normally or at 45°, assuming $m_i/Zm_e=1836\times27/3$ with $m_e=1$ the normalized mass of electrons and Z, the charge number of ions, conservatively assumed to be 3 [10] because of the lack of the experimental data for the simulation conditions at present. Three types of *p*-polarized laser pulses were applied. The amplitude of the leading front of the Gaussian pulse increases from 0.2% of the peak value. Figure 1 shows the dependence of the highest ion energy on the target thickness with laser pulses incident at 45° to the target normal. The open-circle line represents the results for a laser pulse with a focused peak intensity of 1.37×10^{19} W/cm^2 and full width at half maximum (FWHM) duration of 50 fs (i). The solid-circle line is for a 3.5×10^{19} W/cm^2, 50 fs pulse (ii), and the square line is for a 1.37×10^{19} W/cm^2, 100 fs pulse (iii). In case (i), the highest ion energy increases linearly from 0.01 μm to 0.04 μm. After the optimal point the curve first drops rapidly and then slowly, following two distinct scaling laws. For targets with a thickness between 0.04 μm and 0.1 μm, the highest ion energy drops linearly. After 0.1 μm, however, the highest energy decreases exponentially. For cases (ii) and (iii), only the results for the optimal range of thickness is shown in Fig. 1, which is around 0.06 μm. The diamond line in Fig. 1 represents the results of PIC simulations with laser pulses (i), where the effects of binary collisions between electrons and ions are considered. We do not find much difference of the ion acceleration between that with and that without considering the binary collisions. We attribute this to the large mean free path of high-energy electrons in the solid target, which is about 100 μm for 100 keV as calculated [11]. Simulations for *s*-polarized laser pulses incident obliquely or normally on solid foils give much lower ion energies than that for *p* polarization. In the following context, only the results for *p* polarization are shown and discussed.

III. ELECTRON AND ION ACCELERATION

To explain the dependence of the highest ion energy on various target thicknesses, it is necessary to understand the mechanism of the ion acceleration and the electron heating. Figure 2(a) shows the ion momentum spectra for various target thicknesses. The most interesting common feature in the ion momentum spectra is the existence of a high-energy plateau, which ends up with a sharp cutoff typical of the electrostatic ion acceleration mechanism [12]. Another common feature, more obvious for thicker targets, is the presence of peaks in the spectra. The ion momentum spectra in Fig. 2(a) shows that as the target thicknesses increases, the cutoff energy and the effective temperature of the energetic ions decreases. Such a tendency is consistent with the features of the energetic electrons, which produces the electrostatic field locating at the front and the rear of the target, where ions are accelerated, as shown by Dong *et al.* and Wilks *et al.* [13]. The electron energy spectra are shown in Fig. 2(b) for different target thicknesses. It is interesting to point out that for the 0.04 μm target thickness, which is of the optimal thickness for the ion acceleration by applying laser pulses (i), one obtains not only a greater number of energetic electrons but also a higher electron effective temperature than other cases.

As the target becomes thicker, the energetic electron number as well as the effective temperature are dramatically reduced, as for the 0.3-μm and 3-μm targets. For comparison, the bold gray line shows the Maxwellian electron distribution with an effective temperature of 0.74 MeV, corresponding to the ponderomotive potential of the laser $0.511\times(\sqrt{1+\mathbf{a}^2/2}-1)$ MeV, where **a** is the dimensionless vector potential, which is defined as $a^2=I\lambda^2(\mathrm{W/cm^2}\ \mu\mathrm{m}^2)/(1.37\times10^{18})$. Here $a\sim3.16$ in the simulation with $I\lambda^2=1.37\times10^{19}$ W/cm^2 μm^2.

The presence of the two different scaling laws in the decreasing part of the ion highest energy curves in Fig. 1 suggests that there are two different target-thickness regimes. One is the transparent regime (TR), with target thickness less than 0.1 μm. Indeed, with an initial plasma density $n_{e0}=100n_c$, the effective skin depth $\gamma^{1/2}c/\omega_p$ of the target is about 0.025 μm, which increases as the density of the plasma decreases during the interaction. Here, we used $\gamma\sim\sqrt{1+a^2/2}\sim2.54$ and $\omega_p\sim10\omega_0$ with $\omega_p^2=(4\pi e^2n_{e0})/(m)$ and ω_0 the frequency of the plasma and the laser, respectively. The other regime, with target thickness above 0.1 μm, is recognized as the opaque regime (OR). The normalized Hamiltonian of an electron (similar for an ion) is $H=[1+(\mathbf{P}+\mathbf{a})^2]^{1/2}-\phi$, where $\mathbf{P}=\mathbf{p}-\mathbf{a}$ is the canonical momentum of the electron normalized by mc, and ϕ is the charge separation potential normalized here by mc^2/e. m and c are the rest mass of electron and the light velocity in the vacuum, respectively. Physically, the maximum value of ϕ is determined by the total number N_h and the effective temperature T_e of the produced hot electrons, $\phi_{max}\sim f(T_e,N_h)$ [14]. In TR, ϕ includes both the laser-induced electrostatic fields at the front and the rear of the target, whereas in OR ϕ includes only the front part. Such a difference significantly affects the electron acceleration and their angular distribution, as is discussed in the following.

A. Electron stochastic acceleration in TR

For transparent plasmas, laser absorption and electron heating are very strong [15], increasing the electrostatic field that causes ion acceleration [see Figs. 1 and 2(a)]. Figure 3(a) shows the phase space electron distribution when the target is at the optimal thickness of 0.04 μm. The maximum energy of the electrons is above 10 MeV. This energy is much larger than the ponderomotive potential of the laser pulse, which is only $\sim$0.74 MeV. On the other hand, in such a thin target plasma waves cannot develop, so that the model of the electron acceleration by plasma waves cannot account for such a high energy gain. The irregularity of the electron phase distribution in Fig. 3(a) obviously excludes the possibility of the election acceleration by plasma waves. It turns out that the charge separation field in the laser pulse plays a key role in the electron acceleration. The corresponding electrostatic potential bounds the electrons, preventing them from being pushed out of the focusing area before the arrival of the laser pulse peak as shown by Hu and Starace [16]. Figure 3(b) shows the temporal evolution of the longitudinal momentum of a selected typical electron, the laser field and the quasistatic electric field *experienced* by that electron. The

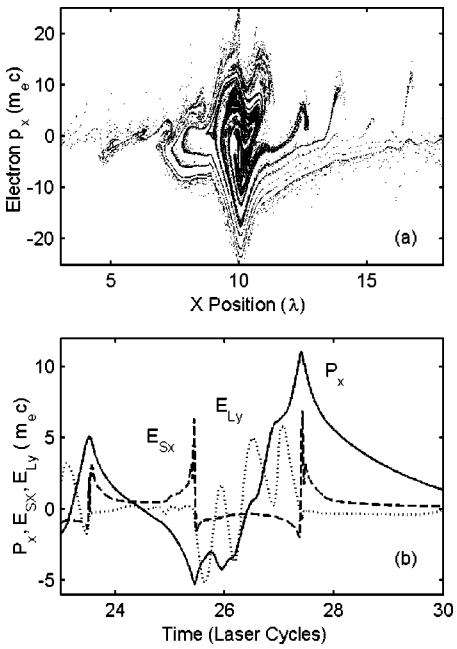

FIG. 3. (a) Phase space of electrons for a 0.04-μm target. (b) Temporal evolution of the longitudinal momentum p_x of a selected electron, the laser electric field E_{ly}, and the laser induced quasistatic electric field E_{sx} *experienced* by that electron, which show how the electron is accelerated.

latter provides instructive information about the acceleration process of that electron. At first, the electron gains energy at the front part of the laser pulse. Meanwhile, it oscillates irregularly, not with laser frequency as expected in a plane electromagnetic wave in the vacuum. At some time, it is stochastically in phase with the laser pulse and then is accelerated to much high energies [17], just as shown during the period between 26.5 and 27.5. After that, the highly energetic electron can either escape from the static electric potential, or continue to oscillate but with a larger phase-space amplitude. It can keep its energy until the end of the laser pulse. We have traced a set of 96 electrons which have $p_x>15$ at the end of the laser pulse and found that 100% of them are accelerated in such a process. Another set of 96 electrons randomly selected were also traced. Among these only four are found to be highly energetic and have experienced the same acceleration process as the first set of 96 electrons. One cannot analyze all the electrons individually in the simulation box in detail, however, it is already obvious that the electron acceleration is due to the existence of the quasistatic electric field at the front and the rear of the target, which destroys the symmetry of the electromagnetic field experienced by the electron as expected in the vacuum, and makes it possible for electrons to be accelerated in the two consecutive half laser cycles. Such acceleration mechanism is also implied in previous works, for instance, in Refs. [16,18].

When the target thickness $d<0.04$ μm, the laser pulse can pass through the plasma with 30% absorption and very little reflection. Electrons in such a foil plasma will have the same acceleration conditions, which results in a similar effective temperature in this regime. The thicker the target is, the more energetic electrons can be produced, i.e., $N_h(d)$

$\propto dn_{e0}$. The electrostatic potential increases linearly with the target thickness, $\phi(d)_{max} \propto d$, so does the highest ion energy as shown in Fig. 1. When the target is thicker than 0.04 μm but still thinner than 0.1 μm, the laser pulse can still propagate through the target, but its energy will be increasingly reflected as the target thickness increases. This dramatically reduces the opportunity for those electrons originally located at or accelerated to the rear of the target to obtain higher energies. The effective temperature of the hot electrons is thus lowered, and in turn also the charge separation potential and the highest energy of ions are reduced, although there are more low-energy electrons due to the larger total number of electrons in thicker targets.

As the intensity and the duration of the incident laser pulse are increased, the optimal thickness increases as shown in Fig. 1. In case (ii) with the laser pulse at a higher intensity but with the same duration, the effective skin depth for the unperturbed target with $n_{e0}=100n_c$ is $\gamma^{1/2}c/\omega_p \simeq 0.031$ μm. During the laser-pulse interaction, however, the thin target expands with time owing to the laser heating and acceleration of target electrons, the average target density is reduced. Therefore, the real effective skin depth should be larger than 0.031 μm. At these simulation conditions, the optimal target thickness for the ion acceleration is found to be about 0.06 μm, almost two times of the skin depth calculated for the unperturbed target density. In case (iii) with a longer laser pulse duration, n_e decreases to a much lower value during the laser-pulse interaction than that in case (i). Moreover, electrons bounded in the electrostatic potential have more chance to encounter the right phase of the laser pulse to gain higher energy in a longer pulse duration. Both of them help to increase the penetration depth when the laser duration increases, which also results in an increased optimal thickness for the ion acceleration. Therefore, the optimal thickness also depends on the pulse duration. Through PIC simulations, we find the optimal target thickness for the ion acceleration is

$$d_{optm} \approx (c/\omega_p)\sqrt{1+\mathbf{a}^2\tau/2}, \tag{1}$$

where τ is the laser pulse duration in units of 50 laser cycles. This means that the optimal thickness is proportional to the pulse energy $a^2\tau$. The difference between increasing the laser intensity and increasing the pulse duration can be seen from the ion acceleration behavior at foil thicknesses below the optimal one. It should be pointed out that Eq. (1) is only valid for experimental conditions with ultrashort intense laser pulses. Once hydrodynamic behavior or parametric instability sets in as with picosecond laser pulses, Eq. (1) becomes invalid.

B. Electron's stochastic acceleration and J×B acceleration in OR

However, as the target becomes opaque (>0.1 μm) in case (i), a large part of the laser energy, for instance, with a target of 3 μm, almost 98%, is reflected. Such low absorption is in contrast with that when 0.04-μm foil is applied. This is also different from PIC simulations by Wilks *et al.* [19]. Wilks *et al.* used a much lower electron density, which makes the intense laser pulse penetrate easily into the plasma, causing great absorption [15].

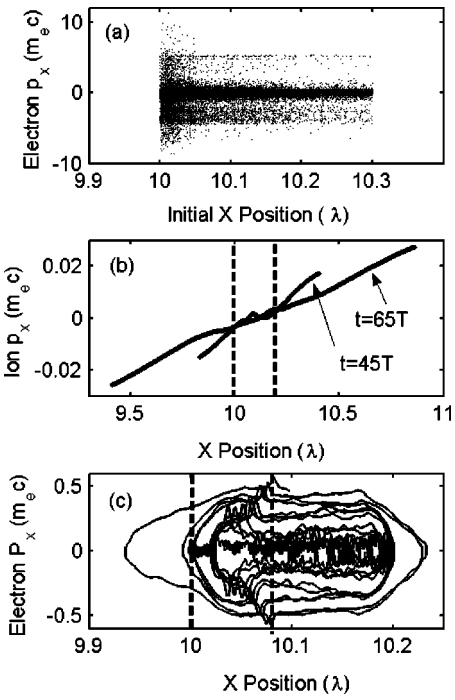

FIG. 4. PIC simulations for 0.3- and 0.2-μm targets. (a) Longitudinal momentum of energetic electrons versus their initial positions at 40 laser cycles. (b) The instantaneous phase space of ions at 45 and 65 laser cycles, respectively. (c) Typical trajectory of an electron, with the area between two dashed lines showing the 0.08 μm penetration depth of the laser pulse.

It is interesting to study the dynamics of electrons. In OR case, we found that the electrostatic field around the rear side of the target now can no longer play roles in accelerating the electrons in the forward direction since the laser light cannot reach there. Figure 4(a) shows the acceleration of electrons at different *initial* positions for the 0.3-μm-thick target at $t=40$ laser periods after the peak of the laser pulse arrives at the surface of the foil. The laser pulse penetrates about 0.08 μm into the target at the end of the laser pulse. Only electrons originally located within the laser penetrating depth can be accelerated to higher energies. Electrons in the remaining part of the target were accelerated to energies up to a cutoff, indicating that the acceleration of this part of electrons at that time may be attributed to the charge separation field located at the front and the rear of the target, where the ions are accelerated as shown by Fig. 4(b). But even in OR, for thin enough targets, hot electrons will be returned to the laser field from the rear of the target and probably accelerated for the second time, enhancing the electron heating to a higher effective temperature than that due to the laser ponderomotive potential alone. The trajectory of one typical electron in the phase space is shown in Fig. 4(c) for a 0.2-μm target. The multiple acceleration behavior of the oscillating electron is obvious. The area between the two dashed lines shows the penetration depth of the laser pulse into the plasma, which is about 0.08 μm. However, for

thicker targets, the accelerated electrons will spend more time in the target. This means that there is little time for them to be accelerated again in the laser pulse. The more time an electron stays in the target, the lower is its energy, and the less its contribution to the electrostatic potential. Comparison [see Fig. 2(b)] between the electron spectra for the 0.3-μm and 3-μm targets shows the effect of the period of electron oscillation on the electron acceleration. In fact, if the target is thick enough, most of electrons will be accelerated only once during the laser pulse.

With thicker targets, the laser-induced electrostatic field is much weaker. The main mechanism of the electron acceleration transforms from the stochastic acceleration to the $\mathbf{J}\times\mathbf{B}$ force acceleration [19]. Therefore, electrons will have a Maxwellian distribution with an effective temperature that is similar to the ponderomotive potential of the laser pulse [19], say 0.74 MeV, as shown in Fig. 2(b) by the thick gray line. One sees that the electron spectrum for the 3-μm target agrees well with the expected distribution for acceleration by the $\mathbf{J}\times\mathbf{B}$ force of the laser pulse. For such a case, with the same or smaller number and the same effective temperature $T_e \simeq 0.74$ MeV of the hot electrons, the effect of the target thickness on the density of electrons leaving the foil determines the variation of the highest ion energy as shown by Mackinon *et al.* [3].

IV. ANGULAR DISTRIBUTION OF ELECTRONS AND IONS

Now we consider the angular distribution of energetic electron and ion emission. Two of us [20] have shown that the angular direction of an accelerated electron is related to its kinetic energy and the local Coulomb potential variation by

$$\tan\theta = \left[\frac{2(\gamma-1)(1+\delta\phi)-\delta\phi^2}{(\gamma-1-\delta\phi)^2}\sin^{-2}\alpha+\tan^{-2}\alpha\right]^{-1/2}, \tag{2}$$

where θ is defined by $\tan\theta = p_y/p_x$, and $\alpha = 45°$ is the incident angle. To derive Eq. (2), one assumes $p_y(t=0) = p_x(t=0) = 0$ and $p_z(t) = 0$, which is generally true both for p and s polarizations. $\delta\phi = \phi(x,t) - \phi_0$ and normalized by mc^2/e, where ϕ_0 is the initial static electric potential and $\phi_0 = 0$ in our case. For ions, $\delta\phi$ should be replaced by $-Zm_e/m_i\delta\phi$. The angular distributions of the forward electrons and ions are shown in Fig. 5 for 0.04-μm and 3-μm targets. One sees that the most energetic electrons are distributed in a narrow cone along the direction (45°) of laser propagation. The Coulomb potential variation experienced by the hot electrons tends to limit their ejecting angles, as shown in Figs. 5(a) and 5(c) for 0.04-μm and 3-μm targets, respectively. For the 0.04-μm target, the hot electrons experience larger Coulomb potential changes, and thus have a wider angular spread for any given energy. In the transparent regime, because the Coulomb field includes the laser-induced electrostatic charge separation fields both at the front and the rear of the target, most of the hot electrons are located in an area limited by $\delta\phi = 1.7$ and 3.4. However, in the opaque regime with 3-μm targets, the electrons locate within the area limited by $\delta\phi = 0$ and 0.4, since here the potential includes only the target-front electrostatic field.

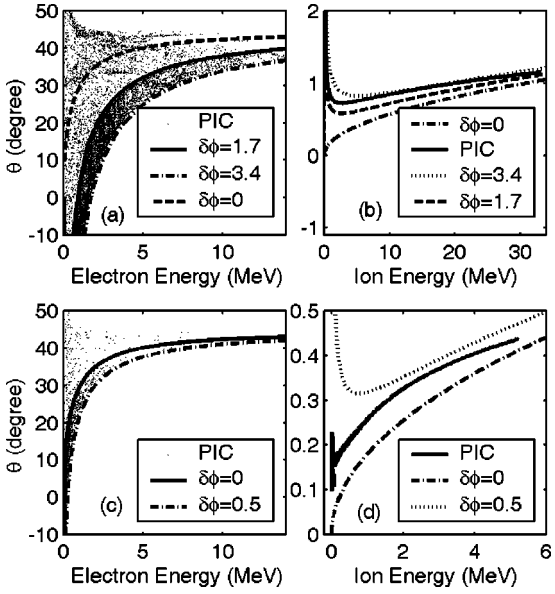

FIG. 5. Angular distribution of energetic electrons and ions for target thickness 0.04 μm [in (a) and (b)] and 3 μm [in (c) and (d)], respectively. $\delta\phi$ is the local Coulomb potential variation experienced by electrons, which is normalized by mc^2/e.

Figures 5(b) and 5(d) show the angular distribution of the ion emission. The ion emission for the 0.04-μm foil is mainly along $\sim 1°$ from the target normal with a FWHM of 2°. As energy increases, the angle increases slightly. The properties of the ion emission indicate that planar electrostatic potentials in the front and the rear of the target are formed. The angular distribution of the energetic electrons and ions appears to show that the electric field is constructed mostly by those not so energetic electrons whose angular distribution spreads to the opposite side to the laser pulse with respect to the target normal and show the characteristic isotropic behavior. However, as shown above by Figs. 1 and 2 in Sec. III, the highest ion energy has the same trend with the energetic electrons and should be related to the number and effective temperature of all the energetic electrons. This apparent discrepancy is removed by taking into account of the electron oscillations in the electrostatic potential. Such behavior is shown clearly in Fig. 3(b). The oscillating energetic electrons stay around the foil target, contributing to the electrostatic field, and therefore play key roles in accelerating ions as shown above.

V. DISCUSSION AND CONCLUSION

One may note that our results of the target optimization for the ion acceleration are obtained with one-dimensional (1D) PIC code, and 2D/3D effects are excluded obviously. One of the 2D/3D effects is the self-generated quasistatic magnetic field that tends to pinch the angular distribution of energetic electrons and expand that of ions [21]. The existence of the strong self-generated magnetic field can also

play important roles in stochastically accelerating electrons [17]. Other 2D/3D effects such as breakup of the laser focus point caused by the fluctuation of the intensity distribution and/or the inhomogeneity of the plasma, can also have effects on the angular distribution of electrons and ions.

We also want to point out that our result is based upon a clean laser-pulse interaction with thin foil targets. To test our predicted optimization, laser pulses with a very high contrast ratio should be applied to avoid the breakup of the thin foil by the prepulses. Such kind of clean laser pulses may be obtained with the optical parametric chirped-pulse amplification technology [22].

In summary, the ion emission in the interactions of intense laser pulses with solid thin foils of sub-micrometer has been investigated using PIC simulations. The narrow angular spread of the energetic ion beam and the optimal ion acceleration curve indicate that such ultrathin foil target can be applied to generate collimated energetic ion beams. The optimal target thickness for the highest ion energy is found to be related to the intensity and the duration of the laser pulse. The enhanced number and effective temperature of hot electrons for a transparent target is responsible for the optimization characteristics of the sub-micrometer foil target.

ACKNOWLEDGMENTS

This work was supported in part by the National Natural Science Foundation of China (Grant Nos. 10105014, 19825110, 10075075), the National Key Basic Research Special Foundation (NKBRSF) under Grant No. G1999075200, and the National High-Tech ICF program.

[1] E. Parra *et al.*, Phys. Rev. E **62**, R5931 (2000); L.M. Chen *et al.*, Phys. Rev. Lett. **87**, 225001 (2001); S. Ter-Avetisyan *et al.*, Phys. Rev. E **64**, 036404 (2001).

[2] J. Zhang *et al.*, Science **276**, 1097 (1997); S. Bastiani *et al.*, Phys. Rev. E **56**, 7179 (1997); P. Zhang *et al.*, *ibid.* **57**, R3746 (1998).

[3] A.J. Mackinnon *et al.*, Phys. Rev. Lett. **88**, 215006 (2002); J. Badziak *et al.*, *ibid.* **87**, 215001 (2001); A. Maksimchuk *et al.*, *ibid.* **84**, 4108 (2000); G. Kulcsàr *et al.*, *ibid.* **84**, 5149 (2000); K. Krushelnick *et al.*, *ibid.* **83**, 737 (1999); A. Forsman *et al.*, Phys. Rev. E **58**, R1248 (1998); M. Lezius *et al.*, Phys. Rev. Lett. **80**, 261 (1998).

[4] T. Ditmire *et al.*, Nature (London) **398**, 489 (1999); J. Zweibak *et al.*, Phys. Rev. Lett. **84**, 2634 (2000).

[5] T. Ditmire *et al.*, Phys. Rev. Lett. **78**, 3121 (1997); T. Ditmire, T. Donnelly, R.W. Falcone, and M.D. Perry, *ibid.* **75**, 3122 (1995).

[6] Y.L. Shao *et al.*, Phys. Rev. Lett. **77**, 3343 (1996); T. Ditmire *et al.*, Nature (London) **386**, 54 (1997).

[7] V. Kumarappan, M. Krishnamurthy, and D. Mathur, Phys. Rev. Lett. **87**, 085005 (2001).

[8] B.-T.V. Vu, A. Szoke, and O.L. Landen, Phys. Rev. Lett. **72**, 3823 (1994); V.J.L. White *et al.*, Phys. Rev. E **49**, R4803 (1994); T. Ditmire *et al.*, Phys. Rev. Lett. **77**, 498 (1996).

[9] M.G. Cadjan and M.F. Ivanov, Phys. Lett. A **236**, 227 (1997).

[10] A. Zhidkov, A. Sasaki, and T. Tajima, Phys. Rev. E **61**, R2224 (2000).

[11] R.J. Harrach and R.E. Kidder, Phys. Rev. A **23**, 887 (1981); H. Teng *et al.*, Phys. Rev. E **67**, 026408 (2003).

[12] V.Y. Bychenkov, V.T. Tikhonchuk, and S.V. Tolokonnikov, JETP **88**, 1137 (1999).

[13] Dong Quan-Li *et al.*, Chin. Phys. Lett. **18**, 796 (2001); S.C. Wilks *et al.*, Phys. Plasmas **8**, 542 (2000).

[14] E.G. Gamaly, Phys. Fluids B **5**, 944 (1993).

[15] E. Lefebvre and G. Bonnaud, Phys. Rev. Lett. **74**, 2002 (1995); J. Fuchs *et al.*, *ibid.* **80**, 2326 (1998).

[16] S.X. Hu and A.F. Starace, Phys. Rev. Lett. **88**, 245003 (2002).

[17] Z.-M. Sheng *et al.*, Phys. Rev. Lett. **88**, 055004 (2002); M.S. Hussein and M.P. Pato, *ibid.* **68**, 1136 (1992); S. Kawata, T. Maruyama, H. Watanabe, and I. Takahashi, *ibid.* **66**, 2072 (1991); S. Kawata *et al.*, Jpn. J. Appl. Phys., Part 2 **29**, L179 (1990).

[18] J. Meyer-ter-Vehn and Z.-M. Sheng, Phys. Plasmas **6**, 641 (1998); A. Pukhov, Z.-M. Sheng, and J. Meyer-ter-Vehn, *ibid.* **6**, 2847 (1999).

[19] S.C. Wilks, W.L. Kruer, M. Tabak, and A.B. Langdon, Phys. Rev. Lett. **69**, 1383 (1992).

[20] Z.M. Sheng *et al.*, Phys. Rev. Lett. **85**, 5340 (2000).

[21] E.L. Clark *et al.*, Phys. Rev. Lett. **84**, 670 (2000), and references therein.

[22] I.N. Ross *et al.*, Opt. Commun. **144**, 125 (1997).